# Transparent Poly(Lactic Acid) Film Crystallized by Annealing beyond Glass Transition Temperature

Ken-ichi Saitou[1,2] and Masayuki Yamaguchi[1)*]

1) School of Materials Science, Japan Advanced Institute of Science and Technology
1-1 Asahidai, Nomi, Ishikawa 923-1292 JAPAN

2) Packaging Technology Laboratory, Kao Corporation
2606 Akabane, Ichikai-Machi, Haga-Gun, Tochigi 321-3497 JAPAN

*Masayuki Yamaguchi, Corresponding author.
E-mail address: m_yama@jaist.ac.jp
Phone: +81-761-51-1621; Fax: +81-761-51-1149

Ken-ichi Saitou
E-mail address: saitou.kenichi4@kao.com

## ABSTRACT

The effect of post-processing annealing beyond the glass transition temperature on optical transparency was studied using poly(lactic acid) (PLA) films containing a nucleating agent such as *N,N'*-ethylenebis(stearamide) (EBS) or *N,N'*-ethylenebis(12-hydroxystearamide) (EBHS). Although the PLA films without the nucleating agent became opaque after exposure to annealing, the film with an appropriate amount of the nucleating agent was found to be transparent (the haze value was lower than 10%). Since the crystallinity was enhanced by annealing, the film showed excellent heat resistance. As compared with EBS, moreover, EBHS had a better capability to produce a transparent film because the aggregates, which appeared during cooling from the molten state, were small. In the case of EBHS, a network structure of fibrous EBHS in molten PLA was confirmed, which was responsible for the reduced size of the PLA crystals and prevented spherulite formation.

Keywords; Poly(lactic acid); Polymer processing; Transparency

## Introduction

In recent years, concern has been increasing rapidly about environmental issues related to plastic packaging materials because most materials used in packaging containers are petroleum-based plastics and are not biodegradable. Besides the depletion of fossil resources and global warming due to $CO_2$ emissions into the atmosphere, illegal dumping will have a negative impact on the ecosystem. This situation is accelerating research and development on plant-derived and biodegradable plastics. Poly(lactic acid) (PLA) is one of the most well-known plant-derived biodegradable resins. Because of its low level of environmental load, much attention has been paid to PLA [1-6]. For example, the rheological properties in the molten state, and thus the processability, were modified by the addition of flexible fine fibers, which provided strain-hardening in transient elongational viscosity [7,8]. Stereo-complex crystals [9] and reactive polymeric modifiers having glycidyl functions [10-12] also have the capability to give strain-hardening in elongational viscosity. The improvement of mechanical toughness has been another major target for research and development because PLA is a brittle material. Besides the conventional method, i.e., rubber addition [13-19], a recent study of the annealing history should be mentioned. According to Huang et al., exposure to annealing near the glass transition temperature $T_g$ improved the mechanical toughness greatly, even without rubber addition, which is attributed to conformational changes of PLA chains [20,21].

When PLA products are obtained by a quenching process, they show very low or no crystallinity, leading to reduced light scattering. Consequently, PLA shows good transparency, which is quite useful for packaging containers that require visibility. However, poor heat resistance owing to its low $T_g$ without crystallization is inevitable [22,23]. It is widely known that the heat resistance of PLA is greatly improved by enhancement of the crystallinity, which is attained by the addition of nucleating agents, including nanofillers and/or plasticizers [1-6,22-29]. Once the crystallinity is enhanced, however, a product usually loses its good transparency because of light scattering.

According to Norris and Stein, the following factors have to be considered when discussing the transparency of a crystalline polymer [30]: (i) light scattering and reflection from surface roughness, impurities, and voids, (ii) light scattering originating from the spherulite texture, and (iii) light scattering due to the polarizability difference of crystalline aggregates. For the last mechanism, the Rayleigh ratio $R(\theta)$ is used to express the scattered intensities as a function of the angle $\theta$ between the direction of the incident light and that of the scattered light by the following equation [30]:

$$R(\theta)=\frac{\langle\eta^2\rangle\pi^2}{\lambda_0{}^4}\left[4\pi\int_0^\infty\frac{\sin(vsr)}{vsr}r^2\gamma(r)\,dr\right] \tag{1}$$

$$v=\frac{2\pi}{\lambda} \tag{2}$$

$$s=2\sin\frac{\theta}{2} \tag{3}$$

where $<\eta^2>$ is the mean-square dielectric constant fluctuation, and $\lambda_0$ and $\lambda$ are the wavelengths of light in a vacuum and medium, respectively. Finally, $\gamma(r)$ is the correlation function describing the correlation between the fluctuations in a vacuum of elements separated by a distance *r*, which is expressed by the following relationship [31]:

$$\gamma(r) = \exp\left(-\frac{r}{a}\right) \tag{4}$$

where *a* is the correlation distance.

As described by these equations, light scattering is pronounced when the correlation distance is in the range of the wavelength of visible light. In other words, light scattering is reduced even for a product having high crystallinity when *a* is much shorter/longer than the wavelength of visible light. In fact, a transparent product of polypropylene (PP) has been developed by addition of a nucleating agent [32-36]. In particular, sorbitol derivatives are well-known nucleating agents, and are called "clarifiers". They are known to form fibrous structures in the PP resin. Then, the crystallization of PP occurs from the surface of fibrous sorbitol derivatives. Under a flow field, the fibrous nucleating agent orients in the flow direction, leading to a high level of orientation of PP chains [37-39]. As a result, the correlation length increases beyond the wavelength of visible light, which is detected in the skin layer of an injection-molded product [33]. Under quiescent conditions, including the core layer in an injection-molded product, the fibrous nucleating agent forms a network structure in a molten resin. Because the mesh size of the network is much smaller than the wavelength of visible light, the size of PP crystals grown from the network surface is small enough to avoid light scattering [33]. Of course, the network structure prevents spherulite formation. Therefore, PP products containing a "clarifier" show good transparency.

Here, we developed a transparent PLA film with high crystallinity, which can be prepared by T-die extrusion, i.e., a common method of film and sheet forming. During T-die extrusion, a molten resin is extruded from a T-shaped die and subsequently quenched by chill rolls. Furthermore, the sheet can be reheated successively after passing through the chill rolls to promote cold crystallization, i.e., crystallization during the reheating process. Considering the productivity in an actual processing operation, however, it is necessary to increase the crystallization rate in the cold-crystallization process. Although numerous studies on the crystallization rate of PLA have been reported, there have been few reports on cold crystallization, and in the existing reports the transparency of the films was not discussed [24,26,40-42].

## Materials

The polymer used to evaluate the crystallinity and transparency was commercially available poly(lactic acid) (PLA) (Ingeo 4032D, NatureWorks, MN, USA) containing 1.40% of the D-isomer. The number- and weight-average molecular weights, evaluated by size exclusion chromatography, were 160,000 and 210,000, respectively, with reference to a polystyrene standard. Furthermore, another poly(lactic acid) containing a large amount of the D-isomer (Sigma-Aldrich, UK) (PDLLA) was employed for rheology measurements. The weight-average molecular weight of PDLLA was 10,000–18,000. As nucleating agents, *N*,*N'*-ethylenebis(stearamide) (EBS) (Itohwax J-550S, Itoh Oil Chemicals, Japan) and *N*,*N'*-ethylenebis(12-hydroxystearamide) (EBHS) (Itohwax J-530, Itoh Oil Chemicals) were used. The chemical structures are given in Figure 1. The sample code indicates the species of the nucleating agent and the weight content. For example, PLA-EBHS-0.5 denotes the PLA sample containing 0.5 wt% of EBHS.

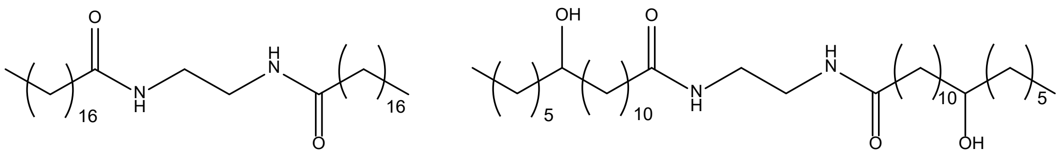


EBS EBHS

**Figure 1.** Chemical structures of EBS and EBHS

**Sample preparation**

Prior to melt mixing, PLA pellets were dried at 110 °C for 3 h. PLA and EBS or EBHS were mixed in a molten state using an internal mixer (Labo Plastmill, Toyo Seiki Seisaku-sho, Japan) for 5 min at 200 °C with a blade rotational speed of 100 rpm. The concentrations of EBHS or EBS were 0, 0.1, 0.3, 0.5, 0.7, 0.9, 1.5, and 2.0 wt%. The obtained mixtures were compressed into flat films of thickness 250 μm by a compression-molding machine (Labo Press, Toyo Seiki Seisaku-sho) at 200 °C under 20 MPa for 120 s, and then quenched at 25 °C for 2 min; the samples are referred to as “quenched films”. Films of relatively high crystallinity were obtained by annealing the quenched films at 100 °C for 2 h.

Besides the blends obtained by internal mixing, other blend samples of PDLLA and the nucleating agent were prepared by manually stirring the mixtures with a spatula in a polytetrafluoroethylene beaker at 200 °C for 5 min. Then the sample was sandwiched between polyimide films (Yupyrex, Ube Industry, Japan) on a hot plate at 200 °C. Thereafter, the film was quenched between metal plates at 25 °C.

**Measurements**

The thermal properties of the PLA films were evaluated using differential scanning calorimetry (DSC) (DSC 8500, PerkinElmer, MA, USA). Approximately 10 mg of the sample, cut out from the sheet, were encapsulated in an aluminum pan. After holding the sample at 200 °C for 10 min, it was quenched to 20 °C at the maximum cooling rate and kept at this temperature for 3 min. Thereafter, the heating run was performed at a rate of 10 °C/min to evaluate the cold-crystallization behavior. The crystallization half time was also measured by DSC. The sample was quenched to 20 °C after melting at 200 °C, and then heated to various crystallization temperatures at the maximum heating rate. The actual heating/cooling rates are shown in the following table.

Table 1 Heating and cooling rates at the DSC measurements

| Start temp. (°C) | 200 | 20 | 20 | 20 | 20 | 20 | 20 |
|---|---|---|---|---|---|---|---|
| End temp. (°C) | 20 | 80 | 90 | 100 | 110 | 120 | 130 |
| Rate (°C/min) | -233 | 169 | 189 | 211 | 225 | 240 | 254 |

The crystallization behavior was examined also by a polarized optical microscope (DMLP, Leica, Germany) equipped with a hot-stage (FP90, Mettler, OH). The quenched films were heated to 100 ºC at 20 ºC/min and kept at the temperatrue to evaluate the isothermal crystallization behavior.

The transparency of the PLA film of thickness 250 μm was measured using a haze meter (LDH 5000, Nippon Denshoku Industries, Japan). The measurements were performed three times and the average value was calculated. Furthermore, light scattering measurements were performed using a helium neon laser with a wavelength of 632.8 nm to evaluate the spherulite texture.

Wide-angle X-ray diffraction (WAXD) patterns of the PLA films were collected with an XRD machine (miniFlex600, Rigaku, Japan) using Cu-Ka radiation at 40 kV and 15 mA. The scanning speed was 10°/min over the $2\theta$ range from 5° to 40°. The measurements were performed three times.

The temperature dependence of the dynamic tensile modulus of the PLA films was evaluated using a dynamic mechanical analyzer (Rheogel E-4000, UBM, Japan). Rectangular samples of width 5 mm and length 20 mm, which were cut out from the compression-molded film of thickness 250 μm, were employed. The samples were heated from room temperature to 180 °C at a heating rate of 2 °C/min. The applied frequency was 1 Hz.

The frequency dependence of the oscillatory shear modulus of the PDLLA samples was measured using a cone-and-plate rheometer (Rheosol G-3000, UBM, Japan) at 100 °C under a nitrogen atmosphere.

The morphology of the nucleating agent was observed by scanning electron microscopy (SEM) (FE-SEM S-4000, Hitachi High-Technologies, Japan). The sample was prepared as follows. First, the PDLLA films annealed at 100 °C were immersed in chloroform at 25 °C. After dissolution of the PDLLA, the solution was filtered using a membrane filter with 1.0 μm pores. The residual materials on the filter were used for the SEM observations after vacuum drying.

The tensile test was performed by a universal tensile machine (AG-IS, Shimazu, Japan) at 25 °C using the dumbbell-shaped specimens cut out from the compressed films (JIS K6251, Number 6). The initial distance between the clamps was 50 mm and one of the clumps moved at a constant speed of 50 mm/min. The measurements were carried out five times for each sample and the average value was calculated.

**Results and Discussion**

Figure 2 shows the DSC heating curves at 10 °C/min for quenched films of PLA and PLA containing 0.5 wt% of the nucleating agent. All the samples clearly show $T_g$ at around 60 °C, suggesting that the quenched samples have low/no crystallinity. It should be noted that a cold-crystallization peak was not observed for neat PLA, although the samples with the nucleating agent had a distinct peak. This result suggested that PLA with the nucleating agent has a number of embryonic crystalline nuclei even after rapid cooling. Therefore, crystallization occurred rapidly once molecular motion was allowed beyond $T_g$. In contrast, pure PLA hardly showed cold crystallization, leading to a small peak at the melting point. The peak cold-crystallization temperatures were 84 °C for PLA-EBHS-0.5 and 87 °C for PLA-EBS-0.5. Furthermore, PLA-EBHS-0.5 gave a sharp peak at the cold-crystallization point, suggesting that EBHS has a better nucleating ability.

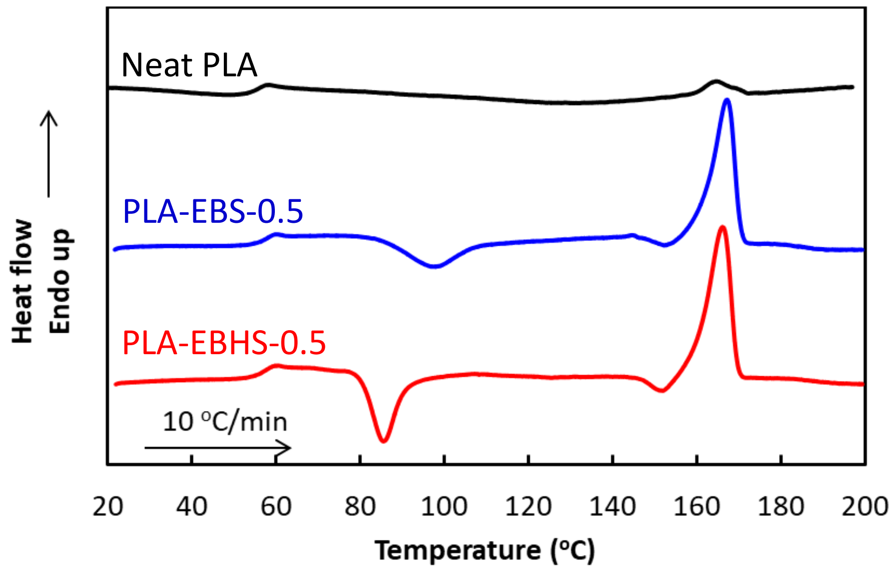


**Figure 2.** DSC heating curves at 10 °C/min after quenching from 200 °C.

The degree of crystallinity ($\chi_c$) of the samples was calculated with equation (1) using the heat of fusion $\Delta H_m$ and exothermic heat of cold crystallization $\Delta H_{cc}$ [21];

$$\chi_c(\%) = \frac{\Delta H_m - \Delta H_{cc}}{\Delta H_{100\%}} \times 100 \qquad (1)$$

where $\Delta H_{100\%}$ is the heat of fusion for a perfect PLA crystal; *i.e.*, 93.1 J/g.

The degrees of crystallinity of PLA, PLA-EBS-0.5, and PLA-EBHS-0.5 were calculated to be 1.4, 3.7, and 6.1 %, respectively.

The crystallization half times at isothermal crystallization are summarized in Figure 3. As seen in the figure, the crystallization half times of PLA-EBHS-0.5 were shorter than those of PLA-EBS-0.5 in the temperature range lower than 110 °C. Since the difference was pronounced at low crystallization temperatures, EBHS is a useful nucleating agent in conventional processing operations in which water is used as the cooling medium. Xing et al. also compared the nucleating abilities of EBS and EBHS, and obtained a similar result [25]. According to them, the hydroxyl groups in EBHS are responsible for the interactions with the carbonyl groups in PLA, which results in a better nucleating ability. At 120 and 130 °C, both samples showed short crystallization half times owing to the enhanced linear growth rate at crystallization. In fact, the linear crystallization rate is known to be maximum at 120 °C for PLA, i.e., the middle of $T_g$ and the equilibrium melting point [22].

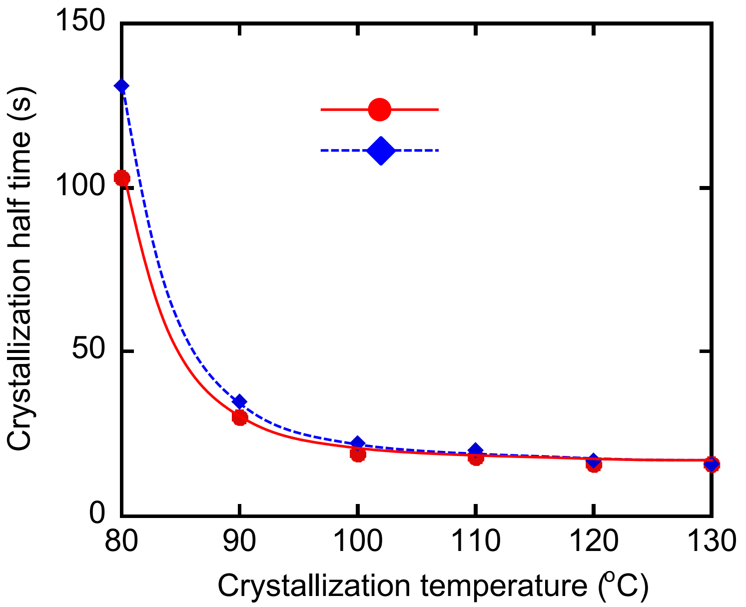


**Figure 3.** Crystallization half times at various crystallization temperatures for (circles) PLA-EBHS-0.5 and (diamonds) PLA-EBS-0.5.

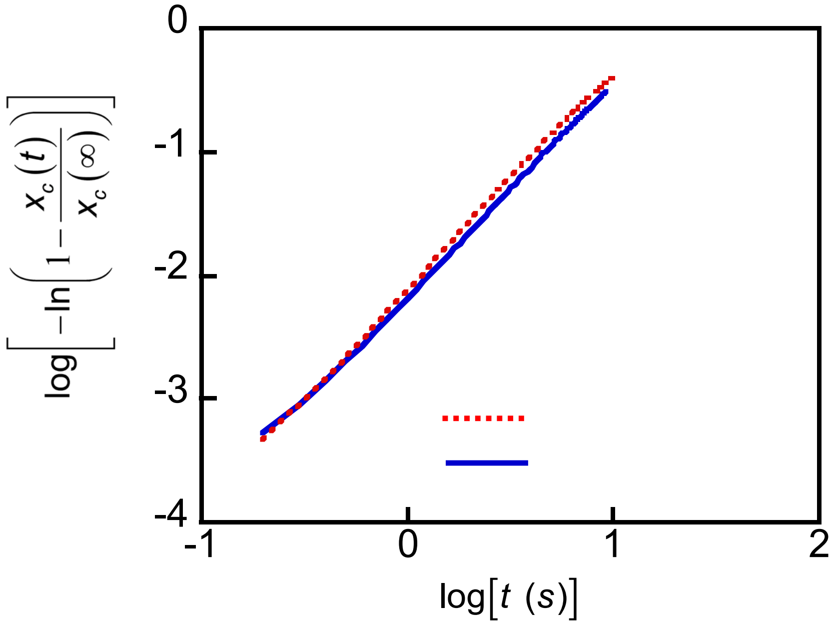


**Figure 4.** Avrami plots for isothermal crystallization at 100 °C for (dotted line) PLA-EBHS-0.5 and (solid line) PLA-EBS-0.5.

The classical Avrami plots are shown in Figure 4, in which $x_c(t)$ is the volume fraction of crystals at time $t$. The crystallization temperature was 100 °C. As seen in the figure, there was no difference in the crystallization kinetics between PLA-EBHS-0.5 and PLA-EBS-0.5.

The crystallization behavior was also studied using a polarizing optical microscope as shown in Figure 5. Before annealing, the samples were optically isotropic at room temperature, and therefore, nothing was detected under crossed polars. This is reasonable because all sample films had low degrees of crystallinity. After annealing at 100 °C for 5 min, which was slightly shorter than the crystallization half time of pure PLA (7.2 min), the difference in the crystalline structure was obvious between the pure PLA film and the films containing the nucleating agents. In the case of the pure PLA film, spherulite texture was clearly detected. In contrast, the crystalline structure was too fine to characterize, which was attributed to a large number of crystalline nuclei.

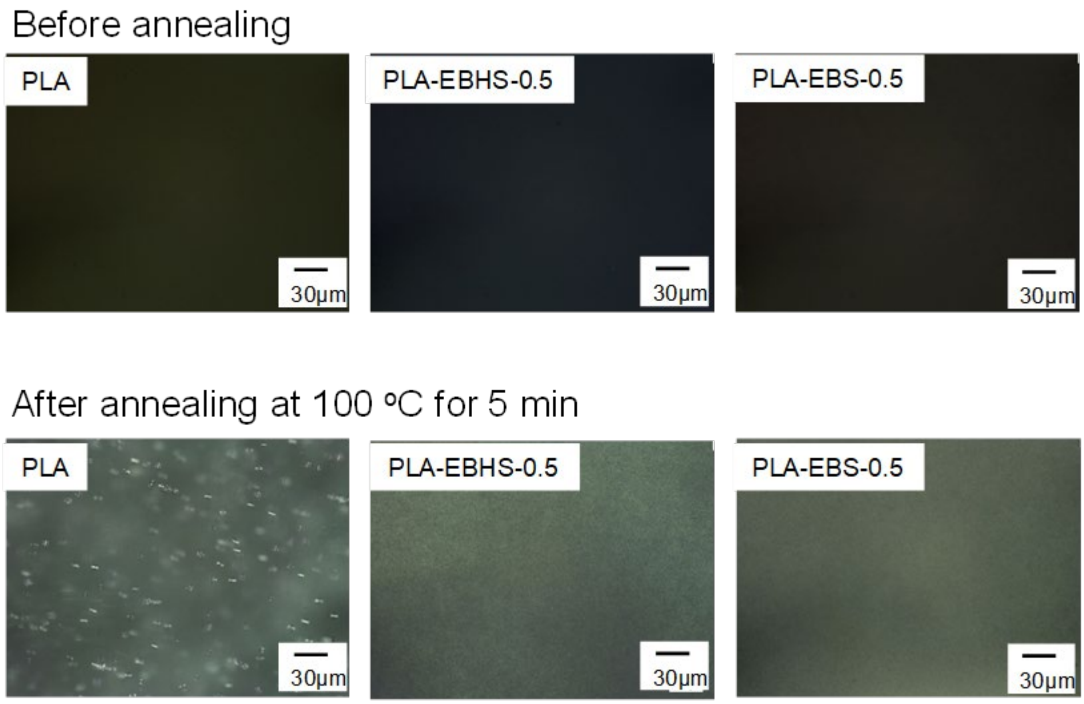


**Figure 5.** Polarized optical photographs under crossed polars for pure PLA, PLA-EBHS-0.5, and PLA-EBS-0.5. (top) Before annealing (quenched films) and (bottom) after annealing at 100 °C for 5 min.

It should be noted that the annealing procedure strongly affected the transparency, as shown in Figure 6. Although the quenched pure PLA film without annealing was transparent (haze value was 1.2 ± 0.1%), it became opaque after exposure to annealing at 100 °C for 2 h (haze value was 76 ± 4%).

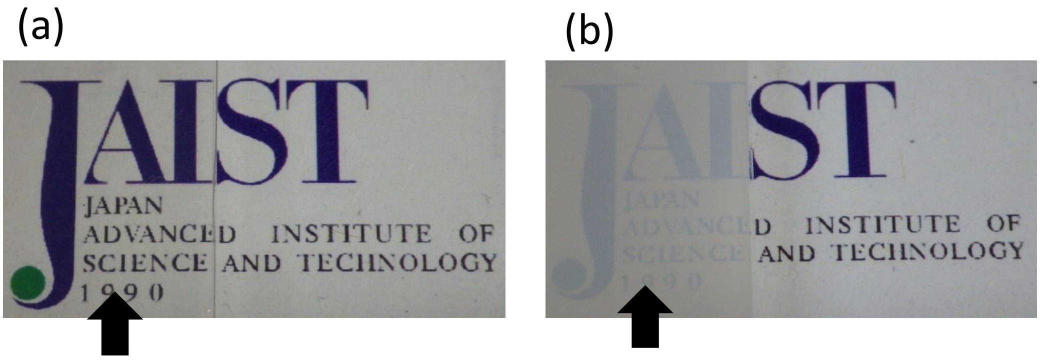


**Figure 6.** Optical photographs of PLA films with 250 μm thickness.

(a) Before annealing (quenched film) and (b) after annealing at 100 °C for 2 h.

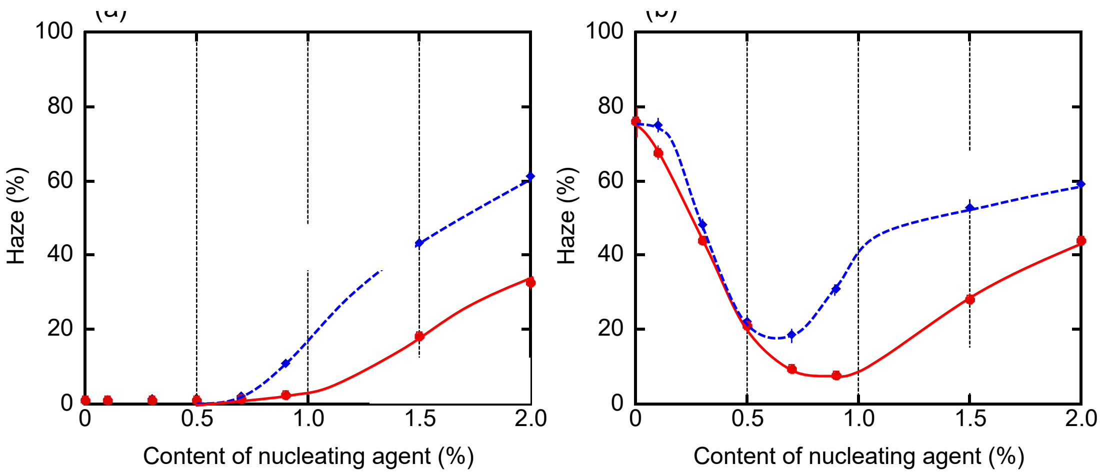


**Figure 7.** Transparencies of PLA films containing (circles) EBHS and (diamonds) EBS. (a) Before annealing (quenched films) and (b) after annealing at 100 °C for 2 h.

The transparencies of the films containing various amounts of the nucleating agent are shown in Figure 7 with error bars. As seen in the figure, the experimental error was significantly small. Therefore, the error bar was not visible in the figure for some points. For the quenched films, the addition of large amounts of the nucleating agents caused the transparency to deteriorate, even without annealing treatment. It was confirmed that no diffraction peaks ascribed to crystals were detected by WAXD measurements for all the films. Compared with the films with EBS, however, those with EBHS exhibited good transparency, indicating that the species of a nucleating agent affected the light scattering originating from its aggregated state in the film, as shown later. It is suggested that EBHS is more uniformly dispersed than EBS in PLA. After exposure to annealing at 100 °C for 2 h, the films became opaque, as shown in Figure 6(b). However, it should be noted that the haze value decreased when the amount of nucleating agent was less than 0.7 wt%. Furthermore, the difference between the effects of EBHS and EBS was obvious when the amount of nucleating agent was greater than 0.7 wt% for both quenched and annealed films.

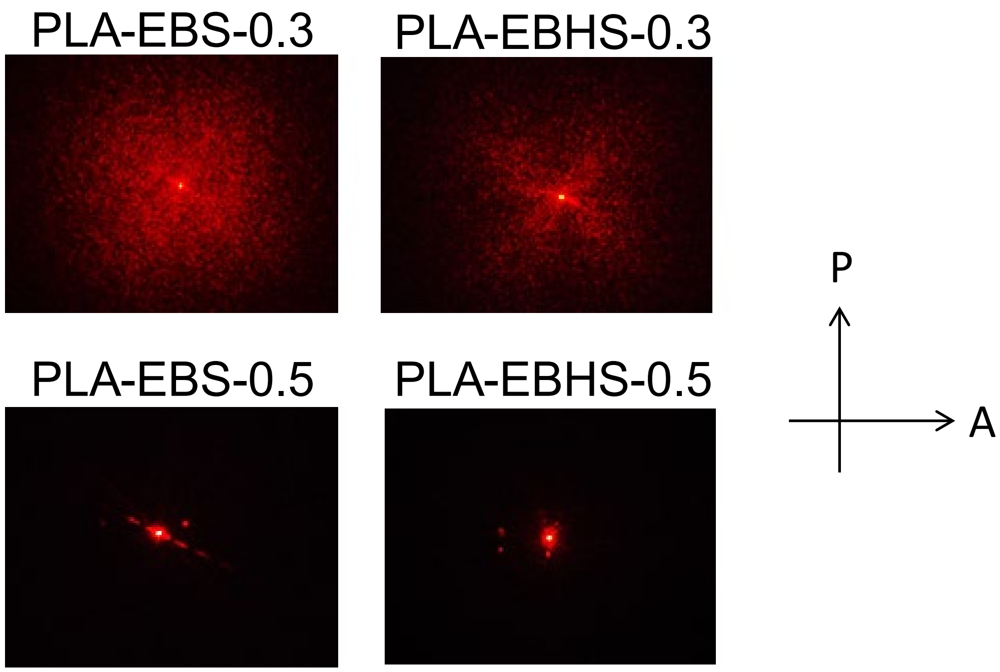


**Figure 8.** HV light scattering patterns of PLA films after annealing at 100 °C for 2 h.

Since light scattering was also caused by the spherulite texture, the HV light scattering images of the annealed films containing the nucleating agent were observed, and are shown in Figure 8. The films with 0.3 wt% of the nucleating agent showed four-leaves patterns, with intense light scattering of the film with EBS. In contrast, the films with 0.5 wt% of the nucleating agent showed almost no light scattering, without four-leaved patterns. The results indicated that addition of the nucleating agent prevented the formation of a spherulite texture.

The WAXD profiles for some annealed films with their degrees of crystallinity $X_c$ are exemplified in Figure 9. The measurements were performed three times for each sample film, and we confirmed that the experimental error of the crystallinity was smaller than 1 %. There was no significant difference in the crystallinity of all the films after annealing, demonstrating that a transparent PLA film with a high degree of crystallinity was successfully obtained by annealing a quenched film containing the specific nucleating agent. The difference in transparency between the films with EBHS and those with EBS can be attributed to the aggregation state of the nucleating agent.

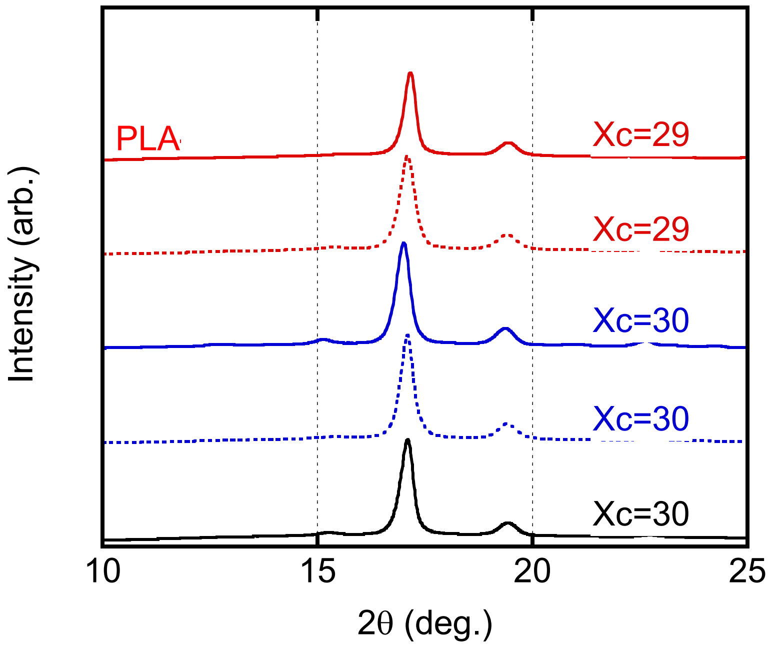


**Figure 9.** WAXD patterns of PLA films annealed at 100 °C for 2 h. The degree of crystallinity $X_c$ (%) is also denoted in the figure.

It is known that a nucleating agent derived from sorbitol, called a “clarifier”, forms a fibrous structure in polypropylene (PP) resin and improves the transparency [32-36]. When the nucleating agent shows aggregation in the resin, however, the aggregates cause light scattering [33].

The performance of the “clarifier” is determined mainly by its nucleating ability and the development of a network structure comprising nanofibrils in the resin. The latter can be evaluated by viscoelastic measurements [32-35]. Therefore, we evaluated the frequency dependence of the oscillatory shear modulus of the resin in the molten state. In this experiment, PDLLA, i.e., an amorphous resin, was employed, to remove the effect of crystals on the viscoelastic properties. The PDLLA used has a low molecular weight, which enabled us to evaluate the long time, i.e., low frequency, region without the effect of reptation of polymer chains. Since the reptation relaxation mode shifted to high frequency because of the low molecular weight, the existence of a network structure, which must appear in the low-frequency region, was easily detected.

As shown in Figure 10, PDLLA showed typical rheological properties in the terminal region, i.e., *G'* and *G"* were proportional to $\omega^2$ and $\omega$, respectively. In contrast, a secondary plateau, which was much lower than the rubbery plateau modulus of PLA [5], appeared in the low-frequency region for samples containing a nucleating agent. The secondary plateau modulus for the sample with EBHS was significantly higher than that with EBS. Considering that both *G'* and *G"* in the high frequency region, i.e., near rubbery region, were not changed greatly by the addition of the nucleating agent, at least EBHS forms a well-developed network structure in the molten resin, similarly to sorbitol derivatives in molten PP [32-35].

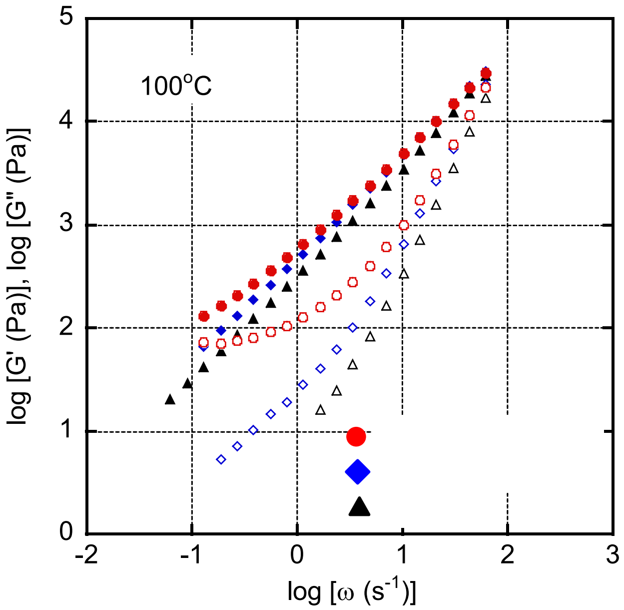


**Figure 10.** Angular frequency dependence of oscillatory shear moduli, namely (open

symbols) storage modulus *G'* and (closed symbols) loss modulus *G"*, at 100 °C for (circles) PDLLA-EBHS-0.5, (diamonds) PDLLA-EBS-0.5, and (triangles) PDLLA.

Moreover, we directly observed the nucleating agent. The PDLLA films with the nucleating agent (0.5 wt%) were washed with chloroform to remove PDLLA. Then, the residual material, i.e., the nucleating agent, was observed by SEM after drying. The SEM images are shown in Figure 11. As seen in the figure, EBHS formed a uniform network structure composed of fibers of diameter ca. 50–100 nm, i.e., smaller than the wavelength of visible light. In contrast, a plate-like structure of width about 100–600 nm was detected for EBS. The result indicated that the size of the nucleating agent aggregate is a critical factor in deciding the transparency, irrespective of the annealing procedure, at least for the films containing more than 0.7 wt% of the nucleating agent. The hydroxyl groups in EBHS presumably play an important role in the self-organization behavior.

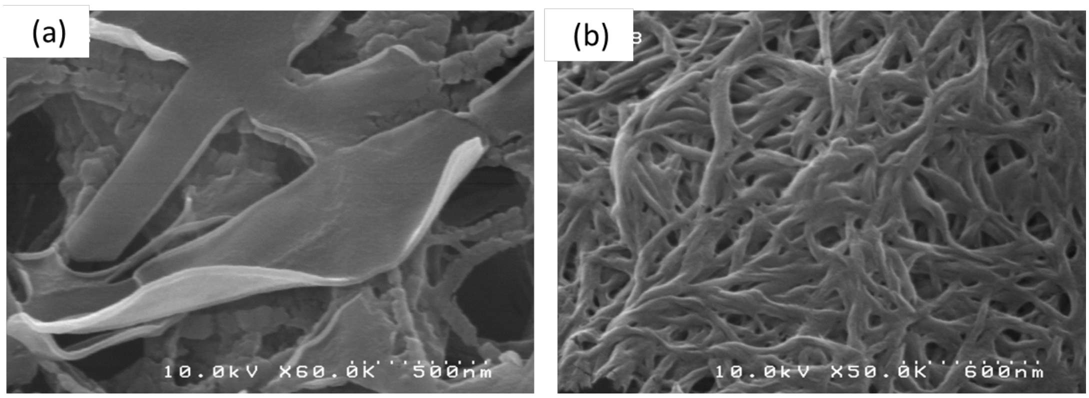


**Figure 11.** SEM images of (a) EBS and (b) EBHS.

Since the fibrous structure was well developed for EBSH, leading to a network structure, high transparency was detected even after cold crystallization. Figure 12 shows the PLA film containing 0.9 wt% of EBHS, i.e., the most transparent film after annealing (haze value was 7.9% ± 0.8%). A comparison with Figure 6(b) shows that the transparency was significantly improved.


**Figure 12.** Optical photograph of PLA-EBHS-0.9 film after annealing at 100 °C for 2 h. The film thickness is 250 μm.

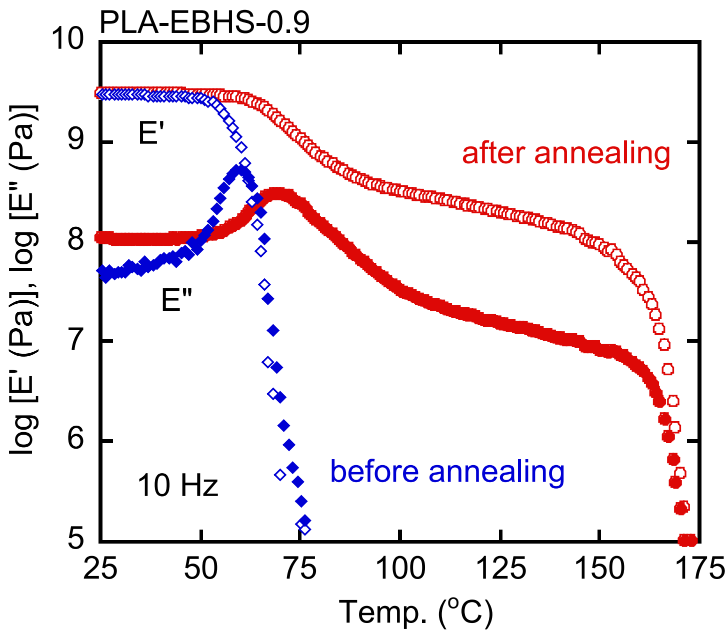

**Figure 13.** Temperature dependence of (open symbols) tensile storage modulus *E'* and (closed symbols) loss modulus *E"* for PLA-EBHS-0.9 (diamonds) without and (circles) with annealing treatment at 100 °C for 2 h.

Figure 13 shows the temperature dependence of the dynamic tensile moduli, i.e., storage modulus *E'* and loss modulus *E"*, for films of PLA-EBHS-0.9. As seen in the figure, the film without the annealing procedure showed an abrupt drop in its modulus at $T_g$, i.e., at around 60 °C. Since the film can be deformed easily near $T_g$, the service temperature was lower than 60 °C. This is a typical phenomenon for quenched PLA films. After exposure to annealing, however, the modulus decreased gradually and fell off at around the melting point. The temperatures to show *E'*= 100 MPa, which can be used as a measure of the heat resistance, were as follows; 65 °C for the pure PLA film and 144 °C for the film of PLA-EBHS-0.9. The result indicates that the heat resistance was greatly improved by the addition of the nucleating agent.

The peak area of *E"* ascribed to the glass-to-rubber transition was reduced with the decrease in the amorphous region, i.e., an increase in the crystallinity. The peak temperature was shifted to a high temperature. This is reasonable because the increase in the crystallinity restricts the motion of amorphous chains, leading to a high $T_g$. After annealing, the dynamic mechanical properties were similar to those of PP, which is known to be a plastic with high heat resistance. Considering that PP is fairly transparent, the annealed PLA film containing EBSH is a good candidate for use as a substitute for PP.

The tensile test was performed to clarify the mechanical properties at room temperature. It was found that all samples exhibited brittle fracture prior to the yielding point, which is usually detected for pure PLA. The initial tensile modulus and tensile strength, i.e., stress at the break point, are summarized in Figure 14 with error bars. After the annealing treatment, both modulus and strength increase slightly, which must be ascribed to the enhanced crystallinity.

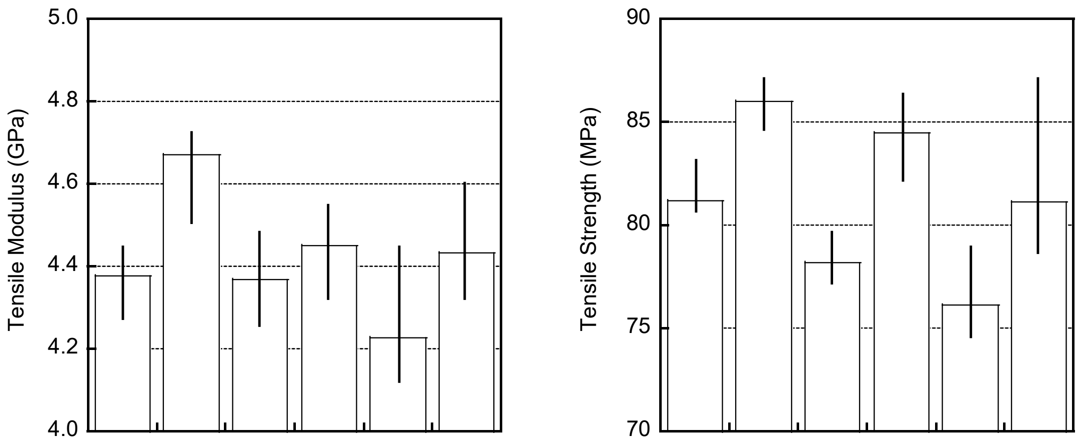


**Figure 14.** Tensile properties such as (a) tensile modulus and (b) tensile strength for PLA, PLA-EBS-05, and PLA-EBHS-0.5 with (A) or without (NA) annealing treatment at 100 °C for 2 h.

This technique, i.e., exposure to annealing for quenched PLA films containing the specific nucleating agent, is suitable for T-die extrusion with equipment consisting of annealing rollers and/or annealing baths after passing through the chill rolls. Since the heat resistance is improved greatly without losing transparency, the products will be preferentially employed in various applications, including packaging containers.

## Conclusion

The structures and properties of PLA films containing a specific nucleating agent were studied, considering the optical transparency and the degree of crystallinity as measures of the heat resistance. In particular, the role of annealing beyond $T_g$ was evaluated using quenched films. The PLA film obtained by a quenching process showed good transparency but no crystallinity. Therefore, the service temperature was lower than 60 °C, i.e., $T_g$. After exposure to annealing at 100 °C for 2 h, the crystallinity was enhanced (ca. 30%). Therefore, the films exhibited excellent heat resistance, although the PLA films lost their transparency. The films containing appropriate amounts of the specific nucleating agent, especially EBHS, however, showed good transparency even after the annealing procedure. The haze values of the films containing 0.7–0.9 wt% of EBHS were lower than 10%, even though the crystallinity was the same as that of the annealed PLA, i.e., good heat resistance. SEM observations of the nucleating agent in the resin and the viscoelastic measurements in the molten state revealed that EBHS exists as fibers of diameter 50–100 nm and forms a network structure. Crystallization on the fibrils of the network reduces the size of the PLA crystals and prevents the growth of a spherulite texture. As a result, a transparent film with high heat resistance is obtained.

## References

1. S.S. Ray, M. Bousmina (2005) Biodegradable polymers and their layered silicate nanocomposites: In greening the 21st century materials world. Prog. Mater Sci 50:

962-1079. https://doi.org/10.1016/j.pmatsci.2005.05.002

2. R. Auras, L.T. Lim, S.E.M. Selke, H. Tsuji (2010) Poly(lactic acid): Synthesis, structures, properties, processing, and applications. Wiley Hoboken.
3. S. Saeidlou, M.A. Huneault, H.B. Li, C.B. Park (2012) Poly(lactic acid) crystallization. Prog Polym Sci 37: 1657-1677. https://doi.org/10.1016/j.progpolymsci.2012.07.005.
4. A. Jimenez, M. Peltzer, R. Ruseckaite (2014) Poly(lactic acid) science and technology: Processing, properties, additives, and applications. RSC Publishing Oxfordshire.
5. M. Yamaguchi (2016) Manufacturing of high-performance biomass-based polyesters by rheological approach, in V.K. Thakur, M.K. Thakur, M.R. Kessler, (Eds.) Handbook of composites from renewable materials. Wiley Hoboken: Chap.2.
6. L.T. Sin, B.S. Tueen (2019) Polylactic acid, 2nd ed. Elsevier Amsterdam.
7. T. Yokohara, S. Nobukawa, M. Yamaguchi (2011) Rheological properties of polymer composites with flexible fine fiber. J Rheol 55: 1205-1218. https://doi.org/10.1122/1.3626414.
8. M. Yamaguchi, T. Yokohara, M.A.B.M. Ali (2013) Effect of flexible fibers on rheological properties of poly(lactic acid) composites under elongational flow. J Soc Rheol Jpn 41: 129-135. https://doi.org/10.1678/rheology.41.129.
9. H. Yamane, K. Sasai, M. Takano, and M. Takahashi (2004) Poly(D-lactic acid) as a rheological modifier of poly(L-lactic acid): Shear and biaxial extensional flow behavior. J Rheol 48: 599-609. https://doi.org/10.1122/1.1687736.
10. M. Yamaguchi, T. Wakabayashi (2006) Rheological properties and processability of chemically modified poly(ethylene terephthalate-co-ethylene isophthalate). Adv Polym Technol 25: 236-241. https://doi.org/10.1002/adv.20078.
11. R. Dhavalikar, M. Yamaguchi, M. Xanthos (2003) Molecular and structural analysis of a triepoxide-modified poly(ethylene terephthalate) from rheological data. J Polym Sci Polym Chem 41: 958-969. https://doi.org/10.1002/pola.10641.
12. L.C. Arruda, M. Magatin, R. E. S. Bretas, M. M. Ueki (2015) Influence of chain

extender on mechanical, thermal and morphological properties of blown films of PLA/PBAT blends. Polym Test 43: 27-37. https://doi.org/10.1016/j.polymertesting.2015.02.005.

13. L. Jiang, M.P. Wolcott, J. Zhang (2006) Study of biodegradable polylactide/poly(butylene adipate-co-terephthalate) blends. Biomacromolecules 7 : 199-207. https://doi.org/10.1021/bm050581q.
14. M. Harada, T. Ohya, K. Iida, H. Hayashi, K. Hirano, H. Fukuda (2007) Increased impact strength of biodegradable poly(lactic acid)/poly(butylene succinate) blend composites by using isocyanate as a reactive processing agent. J Appl Polym Sci 106: 1813–1820. https://doi.org/10.1002/app.26717.
15. T. Yokohara, M. Yamaguchi (2008) Structure and properties for biomass-based polyester blends of PLA and PBS. Eur Polym J 44: 677–685. https://doi.org/10.1016/j.eurpolymj.2008.01.008.
16. N. Zhang, Q. Wang, J. Ren, L (2009) Wang, Preparation and properties of biodegradable poly(lactic acid)/poly(butylene adipate-co-terephthalate) blend with glycidyl methacrylate as reactive processing agent. J Mater Sci 44 : 250-256. https://doi.org/10.1007/s10853-008-3049-4.
17. Y. Li, H. Shimizu (2009) Improvement in toughness of poly(L-lactide) (PLLA) through reactive blending with acrylonitrile-butadiene-styrene copolymer (ABS): Morphology and properties. Eur Polym J 45: 738-746. https://doi.org/10.1016/j.eurpolymj.2008.12.010.
18. D. Kugimoto, S. Kouda, M. Yamaguchi (2019) Improvement of mechanical toughness of poly(lactic acid) by addition of ethylene-vinyl acetate copolymer. Polym Test: in press. https://doi.org/10.1016/j.polymertesting.2019.106021
19. J.J. Han, H.X. Huang (2011) Preparation and characterization of biodegradable polylactide/thermoplastic polyurethane elastomer blends. J Appl Polym Sci 120: 3217-3223. https://doi.org/10.1002/app.33338.
20. T. Huang, M. Miura, S. Nobukawa, M. Yamaguchi (2015) Chain packing and its anomalous effect on mechanical toughness for poly(lactic acid). Biomacromolecules 16: 1660-1666. https://doi.org/10.1021/acs.biomac.5b00293.

21. T. Huang, M. Yamaguchi (2017) Effect of cooling conditions on the mechanical properties of crystalline poly(lactic acid). J Appl Polym Sci 134: 44960-44966. https://doi.org/10.1002/app.44960.
22. T. Huang, M. Miura, S. Nobukawa, M. Yamaguchi (2014) Crystallization behavior and dynamic mechanical properties of poly(L-lactic acid) with poly(ethylene glycol) terminated by benzoate. J Polym Environment 22: 183-189. https://doi.org/10.1007/s10924-014-0638-y.
23. K. Okamoto, T. Ichikawa, T. Yokohara, M. Yamaguchi (2009) Miscibility, Mechanical and Thermal Properties of Poly(lactic acid)/polyester-diol blends. Eur Polym J 45: 2304-2312. https://doi.org/10.1016/j.eurpolymj.2009.05.011.
24. T. Zhaobin, C. Zhang, X. Liu, J. Zhu (2012) The crystallization behavior and mechanical properties of polylactic acid in the presence of a crystal nucleating agent. J Appl Polym Sci 125: 1108-1115. https://doi.org/10.1002/app.34799.
25. Q. Xing, X. Zhang, X. Dong, G. Liu, D. Wang (2012) Low-molecular weight aliphatic amides as nucleating agents for poly (L-lactic acid): Conformation variation induced crystallization enhancement. Polymer 53: 2306-2314. https://doi.org/10.1016/j.polymer.2012.03.034.
26. Z. Xiong, X. Zang, R. Wang, S. Vos, R. Wang, C.A.P. Joziasse, D. Wang (2015) Favorable formation of stereocomplex crystals in poly(L-lactide)/poly(D-lactide) blends by selective nucleation. Polymer 76: 98-104. https://doi.org/10.1016/j.polymer.2015.08.056.
27. L. Aliotta, P. Cinelli, M.B. Coltelli, M.C. Righetti, M. Gazzano, A. Lazzeri (2017) Effect of nucleating agents on crystallinity and properties of poly (lactic acid). Eur Polym J 93: 823-833. https://doi.org/10.1016/j.eurpolymj.2017.04.041
28. Y. Feng, P. Ma, P. Xu, R. Wang, W. Dong, M. Chen, C. Joziasse (2018) The crystallization behavior of poly(lactic acid) with different types of nucleating agents, Intern. J Biological Macromol 106: 955-962. https://doi.org/10.1016/j.ijbiomac.2017.08.095.
29. H. Schüfer, C. Pretschuh, O. Brüggemann (2019) Reduction of cycle times in injection molding of PLA through bio-based nucleating agents. Eur Polym J 115:

6-11. https://doi.org/10.1016/j.eurpolymj.2019.03.011.

30. F.H. Norris, R.S. Stein (1958) The scattering of light from thin polymer films IV. Scattering from oriented polymers. J Polym Sci 22: 87-114. https://doi.org/10.1002/pol.1958.1202711508.
31. P. Debye, A. M. Bueche (1949) Scattering by an inhomogeneous solid. J Appl Phys 20: 518. https://doi.org/10.1063/1.1698419
32. T.A. Shepard, C. Delsorbo, R. Louth, J.L. Walborn, D. A. Norman, N. G. Harvey, R.J (1997) Spontak, Self-organization and polyolefin nucleation efficacy of 1,3;2,4-di-p-dimethylbenzylidene sorbitol. J Polym Sci Part B Polym. Phys 35: 2617-2628. https://doi.org/10.1002/(SICI)1099-0488(19971130)35:16<2617::AID-POLB5>3.0.CO;2-M
33. M. Tenma, M. Yamaguchi (2007) Structure and properties of injection-molded polypropylene with sorbitol-based clarifier. Polym Eng Sci 47: 1441-1446. https://doi.org/10.1002/pen.20839.
34. M. Tenma, N. Mieda, S. Takamatsu, M. Yamaguchi (2008) Structure and properties for transparent polypropylene containing sorbitol-based clarifier. J Polym Sci Part B Polym Phys 46: 41-47. https://doi.org/10.1002/polb.21340.
35. L. Baizano, S. Rastogi, G.W.M. Peters (2008) Flow induced crystallization in isotactic popypropylene -1,3:2,4-bis(3,4-dimethylbenzylidene)sorbitol blends: Implications on morphology of shear and phase separation. Macromolecules 41: 399-408. https://doi.org/10.1021/ma071460g.
36. S. Roy, V. Scionti, S.C. Jana, C. Werdemiotis, A.M. Pischera, M.P. Espe (2011) Sorbitol-POSS interactions on development of isotactic polypropylene composites. Marcomolecules 44: 8064-8079. https://doi.org/10.1021/ma201595j.
37. J. Seemork, M. Siriprumpoonthum, Y. Lee, S. Nobukawa, M. Yamaguchi (2015) Effect of die geometry on drawdown force of polypropylene at capillary extrusion. Adv Polym Technol 34: 21477. https://doi.org/10.1002/adv.21477.
38. P. Phulkerd, T. Nakabayashi, S. Iwasaki, M. Yamaguchi (2018) Enhancement of drawdown force in polypropylene containing nucleating agent. J Appl Polym Sci

136: 47295. https://doi.org/10.1002/app.47295.

39. T. Zhaobin, C. Zhang, X. Liu, J. Zhu (2012) The crystallization behavior and mechanical properties of polylactic acid in the presence of a crystal nucleating agent. J Appl Polym Sci 125: 1108-1115. https://doi.org/10.1002/app.34799.
40. Z. Xiong, X. Zang, R. Wang, S. Vos, R. Wang, C.A.P. Joziasse, D. Wang (2015) Favorable formation of stereocomplex crystals in poly(L-lactide)/poly(D-lactide) blends by selective nucleation. Polymer 76: 98-104. https://doi.org/10.1016/j.polymer.2015.08.056.
41. S. Tomie, N. Tsugawa, M. Yamaguchi (2018) Modifying the thermal and mechanical properties of poly(lactic acid) by adding lithium trifluoromethanesulfonate. J Polym Res 25: 206. https://doi.org/10.1007/s10965-018-1605-4.